Scale Effect on Dropwise Condensation on Superhydrophobic Surfaces

Ching-Wen Lo, Chi-Chuan Wang, and Ming-Chang Lu*

Department of Mechanical Engineering, National Chiao Tung University, Hsinchu, Taiwan

Ⓢ Supporting Information

ABSTRACT: Micro/nano (two-tier) structures are often employed to achieve superhydrophobicity. In condensation, utilizing such a surface is not necessarily advantageous because the macroscopically observed Cassie droplets are usually in fact partial Wenzel in condensation. The increase in contact angle through introducing microstructures on such two-tier roughened surfaces may result in an increase in droplet departure diameter and consequently deteriorate the performance. In the meantime, nanostructure roughened surfaces could potentially yield efficient shedding of liquid droplets, whereas microstructures roughened surfaces often lead to highly pinned Wenzel droplets. To attain efficient shedding of liquid droplets in condensation on a superhydrophobic surface, a Bond number (a dimensionless number for appraising dropwise condensation) and a solid–liquid fraction smaller than 0.1 and 0.3, respectively, are suggested.

KEYWORDS: two-tier roughness, condensation, superhydrophobicity, Cassie droplets, Bond number, solid–liquid fraction
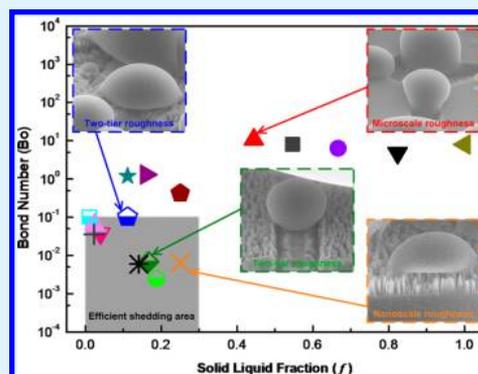
1. INTRODUCTION

Condensation on solid surfaces is a common phenomenon in our daily life and is also widely applied in electronics cooling[1] and industrial systems.[2] Condensate can form Cassie-type droplets[3] or Wenzel-type droplets[4] on solid surfaces. Cassie droplets are suspended on top of structures, whereas Wenzel droplets remain in intimate contact with a solid surface. Cassie droplets that lead to dropwise condensation (DWC) are preferred because DWC offers a superior heat and mass transfer rate than filmwise condensation.[5] Superhydrophobic surfaces feature a liquid contact angle (CA) of approximately 150° or larger and a small contact angle hysteresis (CAH).[6,7] Thereby, DWC can be prompted on such superhydrophobic surfaces.[8] In the past decade, researchers have employed micro- and/or nanostructured surfaces to realize superhydrophobicity in condensation.[9,10] The achievement of superhydrophobicity on microstructured surfaces is the result of the air-pockets formed on the surfaces, which reduces solid–liquid fraction and consequently increases liquid CA.[11] However, it is found that the condensates may penetrate or grow into the microstructures for significant periods and become highly pinned in the microstructures, which can significantly inhibit the mobility of condensates and may deteriorate the heat and mass transfer performance.[12–14] On the other hand, the accomplishment of superhydrophobicity on nanostructured surfaces is primarily due to the large capillary pressure created by the nanostructures, thereby preventing liquid droplets from penetrating into the structures.[15] Besides, micro/nano (two-tier) structure-roughened surfaces comprising both micro- and nanoscale structures have been employed for promoting superhydrophobicity, provided that the microstructures can retain large air

pockets and the nanostructures can simultaneously deliver a large capillary pressure. Although the surfaces with two-tier roughness exhibit a large CA and a small CAH, continuous shedding (including both gravitational droplet removal and coalescence induced droplet jumping) of condensate has been observed only on some of the surfaces,[16–21] whereas highly pinned Wenzel droplets is also encountered on the other surfaces.[22–24] In fact, the macroscopically observed Cassie droplets may have liquid stems underneath the droplets and are actually partial Wenzel.[25–30] The Cassie droplet sits on the top of the micro and/or nano structures, and a liquid bridge is formed at the base of the structure.[31] If the partial Wenzel droplets could be shed efficiently, the high mobility partial Wenzel droplets can exhibit a heat transfer coefficient higher than suspended Cassie droplets due to their more intermediate contact between solid surface and liquid droplet.[25] Studies have also shown that equilibrium CA and CAH are not sufficient for characterizing superhydrophobicity in condensation. The structure size, nucleation site spacing, and droplet size play important roles on wetting state of liquid droplets.[26,27] However, the effect of roughness-scale on the dynamics of condensation process was not addressed. Hence, this work aims to clarify the roughness-scale effect on condensation process subject to superhydrophobic surfaces, and a regime map for efficient shedding of liquid droplets in condensation is developed to clarify the associated influences.

2. EXPERIMENTAL SECTION

In this work, condensation on one-tier and micro/nano (two-tier) structure-roughened surfaces are examined. The surfaces with one-tier roughness being investigated include: silicon nanowire array, parallel microgrooves, and cross microgrooves (denoted hereafter as SiNW, PMG, and CMG, respectively). The surfaces with two-tier roughness examined are parallel microgrooves with silicon nanowire array, and cross microgrooves with silicon nanowire array (denoted hereafter as PMG/SiNW and CMG/SiNW, respectively). The scanning electron microscope (SEM) pictures of the surfaces are shown in Figure 1. The
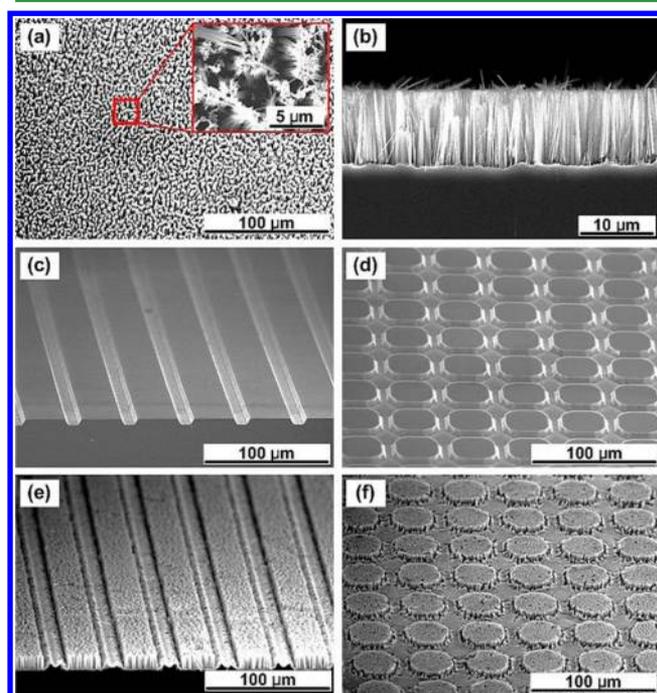
Figure 1. Scanning electron microscope (SEM) pictures depicting: (a) top view of SiNW surface, where the inset is the enlarge view at the selected area; (b) cross-sectional view of SiNW surface; (c) top view of PMG surface; (d) top view of CMG surface; (e) top view of PMG/SiNW surface and (f) top view of CMG/SiNW surface. (3000× magnification in b and 500× magnification in a and c−f.) Images a, b, and e reprinted with permission from ref 17. Copyright 2013 Wiley−VCH.

pictures were taken under the following conditions: 15 kV acceleration voltage, working distance of approximately 10 mm, and emission current of approximately 10 μA. Figure 1a-b show the top view and cross-sectional view of the SiNW, respectively. The inset in Figure 1a is an enlarged view of SiNW. Images c and d in Figure 1 show the top views of PMG and CMG, respectively, whereas images e and f in Figure 1 show the top views of PMG/SiNW and CMG/SiNW, respectively. The SiNW surface comprises nanowires of heights and diameters of approximately 10 μm and 200 nm, respectively. The

PMG surface contains parallel microgrooves. The groove width, spacing, and depth on the PMG surface are approximately 15, 45, and 5 μm, respectively. Meanwhile, the CMG surface has microgrooves along and perpendicular to the gravitational force direction. The groove spacing, width, and depth on CMG are the same as those on the PMG surface. The PMG/SiNW and CMG/SiNW surfaces are made by etching silicon nanowires on the PMG and CMG surfaces, respectively. The fabrication of the microscale structured surfaces was achieved by using KOH etching, whereas the SiNW array was obtained by electroless etching.[17] A thin layer of polytetrafluoroethylene (approximately 20 nm) was coated on top of the studied surfaces by using inductively coupled plasma reactive ion etching to make the surfaces hydrophobic. The equilibrium CAs, advancing CAs, receding CAs, and CAH on these surfaces are provided in Table 1. The equilibrium contact angles were measured using the sessile drop method by DSA-100 (Kruss, Germany) with a liquid droplet volume maintained at 10 μL. The advancing and receding contact angle measurements were performed by filling liquid water into the droplet and retrieving liquid water from the droplet. The error values of the contact angle represent standard deviations of multiple measurements. The equilibrium CAs on the five surfaces are approximately 150°, whereas the values of CAH on the surfaces are distinct. The SiNW, PMG/SiNW, and CMG/SiNW surfaces exhibit a small CAH of approximately or less than 5°, whereas the values of CAH on PMG and CMG surfaces are larger than 60°. This suggests that the silicon nanowires play a significant role on CAH. The equilibrium, advancing, and receding contact angles on the polytetrafluoroethylene-coated plain silicon surface, which are not listed in the table, are 101.8° ± 0.2°, 114.9° ± 0.2°, and 35.2° ± 0.4°, respectively. For PMG and PMG/SiNW surfaces, the contact angles were measured along the groove direction because the grooves are aligned to the gravity direction. The condensation processes on these five surfaces were investigated by using the FEI Quanta 200 environmental scanning electron microscope (ESEM) as shown in Figure 2. The working conditions in ESEM are 15 kV acceleration voltage, working distance of approximately 8.8 mm, emission current of approximately 10 μA, and scanning rate of 4 frames per second. It is noted that the scanning time has been maintained to be smaller than 1 min to eliminate the charging effect on condensation,[17] and a large scanning area (approximately 340 × 180 μm^2) was used to diminish the heating effect.[32] In the experiments, the surfaces were kept at a tilt angle of 45°, and the vapor pressure and temperature of the cooling stage in the ESEM chamber were kept constant at 6 Torr and 0 °C, respectively. The test section in the ESEM chamber for conducting the experiments is similar to that in our previous work.[17] The supersaturation (defined as the ratio of the vapor pressure to the saturation pressure corresponding to the temperature of condensing surface) is maintained at approximately 1.3 to study the effect of roughness scale on condensation. For the effect of supersaturation, readers are referred to the literature.[5,27,33]

3. RESULTS AND DISCUSSION

3.1. Visualization of Dropwise Condensation under ESEM.
Figure 2a−e shows the condensation processes on SiNW, PMG, CMG, PMG/SiNW, and CMG/SiNW surfaces, respectively. The liquid droplets are randomly distributed on

Table 1. Contact Angle Measurements on Various Surfaces[a]

sample	contact angle (deg)				
	SiNW	PMG	CMG	PMG/SiNW	CMG/SiNW
θ_{eq}	144.3 ± 0.2	140.7 ± 0.1	141.6 ± 0.1	145.3 ± 0.2	154.3 ± 0.3
θ_{adv}	146.7 ± 0.4	143.7 ± 0.8	156 ± 0.6	147 ± 0.2	155.6 ± 1
θ_{rec}	141.8 ± 0.6	81 ± 7.4	80.1 ± 8.1	145.6 ± 0.1	155.3 ± 0.1
θ_{hys}	~4.9	~63	~76	~1.4	~2.3

[a]θ_{eq}, θ_{adv}, θ_{rec}, and θ_{hys} refer to macroscopic equilibrium contact angle, advancing contact angle, receding contact angle, and contact angle hysteresis, respectively, on the SiNW, PMG, CMG, PMG/SiNW, and CMG/SiNW surfaces.
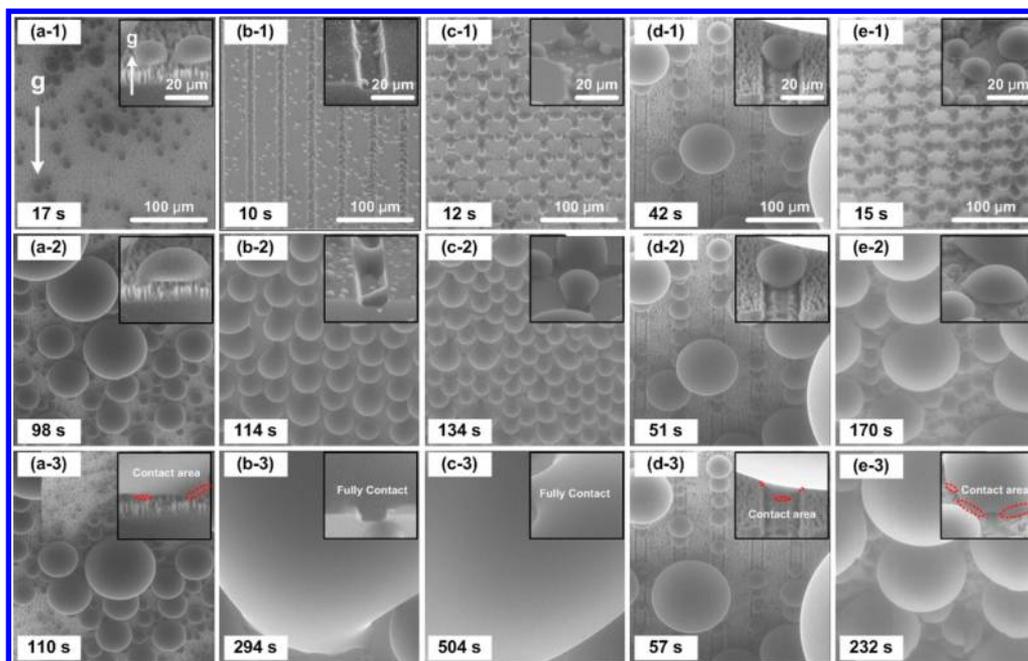
Figure 2. Environmental scanning electron microscopic (ESEM) pictures showing the dynamics of the condensation processes on (a) SiNW surface, (b) PMG surface, (c) CMG surface, (d) PMG/SiNW surface, and (e) CMG/SiNW surface (800× magnification). The inset figures are the enlarged views with 6000× magnification. The red dash lines in the insets in a-3, d-3, and e-3 represent the actual solid−liquid contact area for the partial Wenzel droplets. Images in a and d reprinted with permission from ref 17. Copyright 2013 Wiley−VCH.
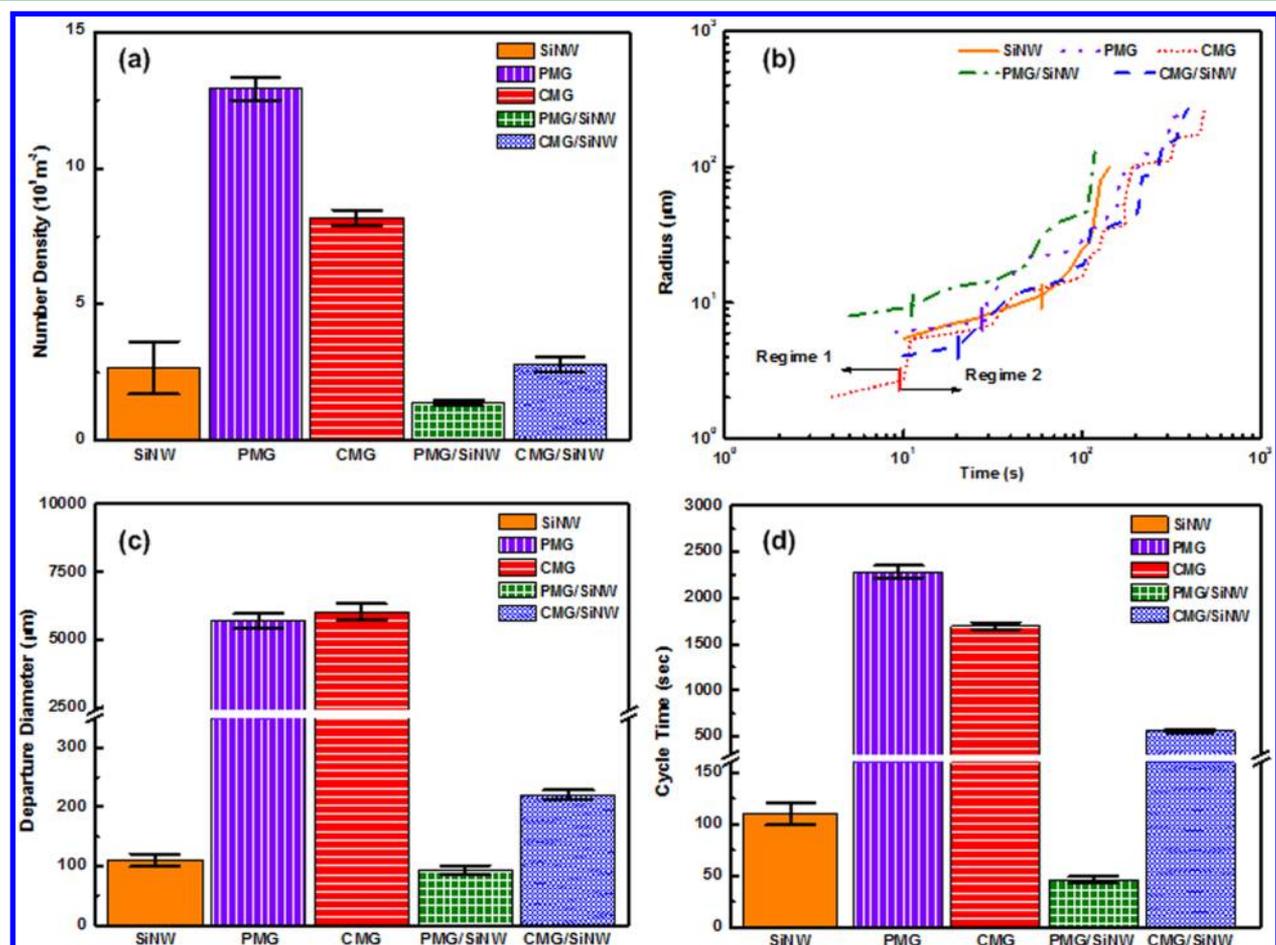
Figure 3. Quantitative analysis of the condensation processes on SiNW, PMG, CMG, PMG/SiNW, and CMG/SiNW surfaces: (a) number density, (b) droplet radius as a function of time, (c) departure diameter, and (d) cycle time.

SiNW, PMG, and CMG surfaces as seen in Figure 2a-1, b-1, and c-1, whereas droplets nucleate at microgrooves on PMG/SiNW and CMG/SiNW surfaces as found in Figure 2d-1 and e-1. The spatial control of heterogeneous nucleation on the two-tier structure-roughened surfaces (i.e., PMG/SiNW and CMG/SiNW surfaces) is analogous to that observed in our previous work.[17] It is also noted that the grooves on the PMG and CMG surfaces are too large as compared to the size of equilibrium droplet radius, which is on the order of a few nanometers.[17] Consequently, no scale effect on heterogeneous nucleation is observed on the PMG and CMG surfaces. Figure 2a-2, b-2, c-2, d-2, and e-2 show the condensation images at a later time after droplet nucleation. Continuous shedding of liquid droplets has only been found on SiNW, PMG/SiNW, and CMG/SiNW surfaces, whereas highly pinned Wenzel droplets are observed on PMG and CMG surfaces as shown in Figure 2a-3, b-3, c-3, d-3, and e-3. The insets in Figure 2 show the enlarged views of the condensation processes on the surfaces. The liquid droplets which nucleate at microgrooves on the PMG and CMG surfaces bridge the grooves rapidly (see insets in Figure 2b-2, c-2) and form Wenzel droplets thereafter, resulting in the highly pinned Wenzel droplets on PMG and CMG surfaces. The enlarged views of the condensation processes on SiNW, PMG/SiNW, and CMG/SiNW (shown in the insets in Figurs 2a-3, d-3, e-3) show that the observed macroscopic Cassie droplets are actually partial Wenzel, having liquid stems in the NWs, which is similar to that observed by Miljkovic et al.[25] This is consistent with the regime map of wetting state using a length ratio of 3.4 on the silicon nanowire array-coated surfaces.[27] The length ratio is the ratio of mean droplet-separation distance ($\sim 17~\mu$m) to microcavity spacing ($\sim 5~\mu$m). Note that the high aspect ratio and small feature size of the NWs can promote super-hydrophobicity,[34,35] which is evidenced by the observed large CAs and small CAHs on the nanowire array-coated surfaces. However, despite that the CAs and CAHs on the SiNW, PMG/SiNW, and CMG/SiNW are approximately the same; the departure diameter on CMG/SiNW surface is much larger than those on SiNW and PMG/SiNW surfaces. The larger liquid-stem area found on the CMG/SiNW surface is presumably responsible for the stickier droplet and the large departure diameter on the CMG/SiNW surface.

3.2. Quantitative Analysis of the Condensation Processes. Quantitative analysis of the condensation processes is shown in Figure 3. Figure 3a−d present the results of the nucleation site density, growth rate, departure diameter, and cycle time, respectively, on the surfaces. At least three experiments have been conducted to obtain the mean values shown in Figure 3. The relative uncertainties of the measurements estimated from error propagation theory are smaller than the standard errors of multiple measurements and the error bars in the figure represent the standard errors. Figure 3a shows the nucleation site densities on the surfaces. They are determined from counting the number of droplets in the first recordable ESEM images (i.e., Figure 2a-1, b-1, c-1, d-1, and e-1) in a fixed area (approximately $340 \times 180~\mu m^2$). The nanowire array-covered surfaces (i.e., SiNW, PMG/SiNW, and CMG/SiNW) exhibit a smaller nucleation site density than PMG and CMG surfaces because the small-sized cavities between the nanowires give a larger free energy barrier for nucleation. The equilibrium droplet radius determined from Kelvin and Clapeyron equation is 3.2 nm using the experimental conditions.[17] Furthermore, from the classical nucleation theory, the free energy barriers to nucleation on the

microgrooves, the microcavities on the nanowire array, and the space between nanowires having characteristic sizes of 15 μm, 5 μm, and 200 nm, respectively, are -2.07×10^{-10} J, -2.27×10^{-11} J and -2.8×10^{-14} J, respectively.[17] Consequently, a relatively large number of embryos were observed on the microgrooves-patterned surfaces (i.e., PMG and CMG surfaces).

The evolution of liquid droplets on the surfaces is shown in Figure 3b. The exponents of te growth rate (α) of the liquid droplets ($r \propto t^{\alpha}$) are summarized in Table 2. The growth of

Table 2. Growth Dynamics^a

sample ID	regime 1	regime 2
SiNW	0.41	1.38
PMG	0.52	1.71
CMG	0.5	1.22
PMG/SiNW	0.38	0.68
CMG/SiNW	0.42	2.21

^{a}The exponents (α) of the growth rate power law ($r \propto t^{\alpha}$) on various surfaces

liquid droplets can be generally classified into two regimes. In the first regime, isolated growth of liquid droplets is observed, and the α values on these surfaces range from 0.38 to 0.52. In the second regime, the growth of liquid droplets is contributed from both isolated droplet growth and coalescence of liquid droplets. This results in considerable rise of α values to 1.38, 1.71, 1.22, 0.68, and 2.21 on SiNW, PMG, CMG, PMG/SiNW, and CMG/SiNW surfaces, respectively.

The departure diameters of liquid droplets are shown in Figure 3c. The departure diameters on the SiNW and PMG/SiNW surfaces were measured by averaging the diameters of droplets shown in the ESEM images. The departure diameters on the PMG, CMG, and CMG/SiNW surfaces are too large to be recorded from the ESEM images. Thus, they were estimated from a theoretical calculation based on force balance (see Figure S1 in the Supporting Information for detail). Note that because the actual solid−liquid contact area in partial Wenzel droplets plays an important role on droplet dynamics, a factor X defined as the ratio of actual solid−liquid contact area to the solid surface area underneath the droplet for partial Wenzel droplets is introduced in the theoretical calculation (see Table S1 in the Supporting Information for the values of X). The SiNW and PMG/SiNW surfaces have small droplet departure diameters as compared to the other surfaces. The large solid−liquid contact areas on PMG, CMG, and CMG/SiNW surfaces lead to the stickier droplets and the larger departure diameters on the surfaces.

The cycle time representing the time required for a cycle from nucleation to departure of a liquid droplet is shown in Figure 3d. The cycle times of liquid droplets on SiNW and PMG/SiNW surfaces were determined from the ESEM images shown in Figure 2, whereas the cycle times on PMG, CMG, and CMG/SiNW surfaces were estimated from the theoretically calculated departure diameters and the growth rates in Figure 2b. A small cycle time suggests a better heat and mass transfer rate.[17] The SiNW surface offers an order of magnitude smaller cycle time than those on the PMG and CMG surfaces. The surfaces with two-tier roughness do not necessarily yield better performance. The PMG/SiNW surface exhibits the smallest cycle time but the cycle time on CMG/SiNW surface is large. The large solid−liquid contact areas of the partial
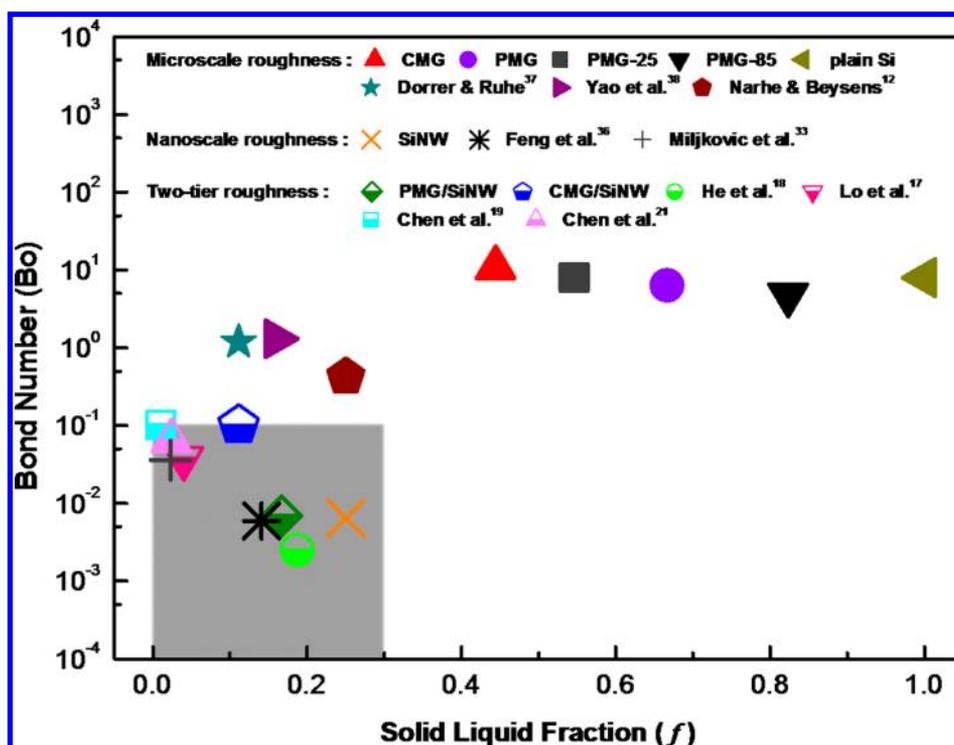
Figure 4. Nondimensional map showing the Bond number as a function of solid−liquid fraction (f). Efficient shedding of the condensates is observed in the gray area in the figure with $Bo \leq 0.1$ and $f < 0.3$.

Wenzel droplets on CMG/SiNW surface are responsible for the large cycle time on the surface.

3.3. Nondimensional Analysis. Notice that surfaces with two-tier roughness are often considered to perform better in shedding behavior because the solid−liquid fraction (f) for Cassie droplets (i.e., $\cos\theta_{CB} = f(\cos\theta_0 + 1) − 1$, where θ_{CB} and θ_0 are Cassie CA and equilibrium CA, respectively[3]) is reduced, thereby resulting in a larger Cassie CA. However, condensation that is a multiscale process includes heterogeneous nucleation, growth, and departure of liquid droplets. Therefore, the macroscopically observed Cassie droplets often have liquid stems underneath them and are actually partial Wenzel droplets. As a consequence, the actual solid−liquid contact area is responsible for the droplet dynamics in condensation. To further elucidate the idea, we performed a nondimensional analysis. A modified Bond number denoting the ratio of gravitational force to the surface tension force is defined as

$$Bo = \frac{\rho g D^2}{\sigma f} \tag{1}$$

where σ is surface tension, f is the solid−liquid fraction for Cassie droplet, ρ is the density of liquid, g is gravity, and D is the averaged departure diameter of droplets (including both gravitational droplet removal and coalescence induced droplet jumping) on a surface. The derivation of eq 1 can be found in the Supporting Information. A small Bond number is preferred because liquid droplets are more likely to be suspended on structures by the capillary force provided by the structures. A nondimensional map showing the Bond number vs the solid−liquid fraction (f) is presented in Figure 4. The map includes our results and some of the condensation results in previous studies.[12,17−19,21,33,36−38] It is noted that structure aspect ratio on a surface affects the wetting state of liquid droplets on the surface,[27] which eventually determine the droplet departure diameters and Bond numbers on the surface. Thus, the effect of structure aspect ratio is implicitly included in the regime map. The PMG-85 and PMG-25 surfaces in the figure represent parallel microgrooves having groove spacings of 85 and 25 μm, respectively. The SEM and ESEM images for the PMG-85, PMG-25 and plain Si surfaces are shown in Figure S3 and Figure S4, respectively, in the Supporting Information. The departure diameters on the surfaces cannot be recorded from the ESEM images directly due to the observational limitation. Thus, they were estimated using eq S3 in the Supporting Information. The obtained departure diameters on PMG-85, PMG-25, and plain Si surfaces are 5.5, 5.8, and 7.8 mm, respectively. A large Bond number ($Bo \geq 0.5$) is found on the microstructure-roughened surfaces, i.e., PMG, CMG, PMG-85, PMG-25, and the surfaces studied by Narhe and Beysens,[12] Dorrer and Rühe,[37] and Yao et al.,[38] as well as on the plain Si surface. Eventually, highly pinned Wenzel droplets is observed on these surfaces. On the other hand, a very small Bond number ($Bo \leq 0.01$) is observed on the nanostructure-roughened surfaces, i.e., SiNW and the surfaces studied by Feng et al.,[36] and on some of the surfaces with two-tier roughness, i.e., PMG/SiNW and the surface studied by He et al.[18] The solid−liquid fractions on these surfaces (i.e., SiNW, PMG/SiNW, and the surfaces studied by He et al.[18] and Feng et al.[36]) are between 0.1 and 0.3. Moreover, the nanostructure-roughened surface,[33] and the two-tier roughened surfaces, i.e., CMG/SiNW and the surfaces studied by Lo et al.,[17] Chen et al.,[19] and Chen et al.,[21] in spite of having a small solid−liquid fraction ($f < 0.1$), exhibit a relatively large Bond number ($0.01 \leq Bo \leq 1$). The small solid−liquid fraction on the nanostructure-roughened surface results in the decrease of the capillary force and leads to the large Bond number on the surface. In the meantime, the decrease of solid−liquid fraction by introducing microstructures on the two-tier roughened

surfaces (i.e., CMG/SiNW and the surfaces in Lo et al.,[17] Chen et al.,[19] and Chen et al.[21]) results in an increase of actual solid−liquid contact area as well. This causes the increase of the departure diameter in the numerator of the Bond number for the surfaces with two-tier roughness. Thus, surfaces with two-tier roughness do not necessarily perform well in condensation. It is worth noting that previous study had shown that a critical solid−liquid fraction of $f < 0.1$ would result in droplet jumping motion.[39] From the nondimensional map, to maintain efficient removal of liquid droplets with a departure diameter being smaller than 100 μm, a Bond number and a solid liquid fraction (f) smaller than 0.1 and 0.3, respectively, are recommended. The conclusion is helpful for designing superhydrophobic surfaces in real applications, such as vehicle windshields or bathrooms.

4. CONCLUSIONS

Scale effect of surface roughness on condensation was systematically studied. Nanostructure and micro/nano (two-tier) structure-roughened surfaces could potentially offer efficient DWC, whereas microstructure-roughened surfaces often lead to highly pinned Wenzel droplets in condensation. It should be noted that not all the surfaces with two-tier roughness perform well in condensation because the introduction of microstructure on the surfaces may eventually result in an increase of departure diameter. To achieve an efficient DWC, we suggest a Bond number and a solid−liquid fraction smaller than 0.1 and 0.3.

ASSOCIATED CONTENT

Ⓢ Supporting Information

Theoretical calculation of the departure diameter of the liquid droplets; solid−liquid fractions of partial Wenzel droplets; derivation of the modified Bond number; SEM and ESEM images of the PMG-85, PMG-25, and plain Si surfaces. This material is available free of charge via the Internet at http://pubs.acs.org/.

AUTHOR INFORMATION

Corresponding Author
*E-mail: mclu@mail.nctu.edu.tw.

Notes
The authors declare no competing financial interest.

ACKNOWLEDGMENTS

REFERENCES

(1) Carey, V. P. *Liquid-Vapor Phase-Change Phenomena*, 2nd ed.; CRC Press: Boca Raton, FL, 2008; pp 413−468.

(2) Cengel, Y. A.; Boles, M. A. *Thermodynamics: An Engineering Approach*; McGraw-Hill: New York, 2008; pp 497−622.

(3) Cassie, A. B. D.; Baxter, S. Wettability of Porous Surfaces. *Trans. Faraday Soc.* **1944**, *40*, 546−551.

(4) Wenzel, R. N. Resistance of Solid Surfaces to Wetting by Water. *Ind. Eng. Chem.* **1936**, *28*, 988−994.

(5) Rose, J. W. Dropwise Condensation Theory and Experiment: A Review. *Proc. Inst. Mech. Eng. A J. Power* **2002**, *216*, 115−128.

(6) Nakajima, A.; Fujishima, A.; Hashimoto, K.; Watanabe, T. Preparation of Transparent Superhydrophobic Boehmite and Silica Films by Sublimation of Aluminum Acetylacetonate. *Adv. Mater.* **1999**, *11*, 1365−1368.

(7) Sun, T.; Feng, L.; Gao, X.; Jiang, L. Bioinspired Surfaces with Special Wettability. *Acc. Chem. Res.* **2005**, *38*, 644−652.

(8) Patankar, N. A. Supernucleating Surfaces for Nucleate Boiling and Dropwise Condensation Heat Transfer. *Soft Matter* **2010**, *6*, 1613−1620.

(9) Yan, Y. Y.; Gao, N.; Barthlott, W. Mimicking Natural Superhydrophobic Surfaces and Grasping the Wetting Process: A Review on Recent Progress in Preparing Superhydrophobic Surfaces. *Advances in Colloid and Interface Science* **2011**, *169*, 80−105.

(10) Celia, E.; Darmanin, T.; Taffin de Givenchy, E.; Amigoni, S.; Guittard, F. Recent Advances in Designing Superhydrophobic Surfaces. *J. Colloid Interface Sci.* **2013**, *402*, 1−18.

(11) Quéré, D. Non-Sticking Drops. *Rep. Prog. Phys.* **2005**, *68*, 2495−2532.

(12) Narhe, R. D.; Beysens, D. A. Growth Dynamics of Water Drops on a Square-Pattern Rough Hydrophbic Surface. *Langmuir* **2007**, *23*, 6486−6489.

(13) Narhe, R. D.; Beysens, D. A. Nucleation and Growth on a Superhydrophobic Grooved Surface. *Phys. Rev. Lett.* **2004**, *93*, 076103−1−4.

(14) Lafuma, A.; Quere, D. Superhydrophobic States. *Nat. Mater.* **2003**, *2*, 457−460.

(15) Kwon, H.-M.; Paxson, A. T.; Varanasi, K. K.; Patankar, N. A. Rapid Deceleration-Driven Wetting Transition During Pendant Drop Deposition on Superhydrophobic Surfaces. *Phys. Rev. Lett.* **2011**, *106*, 036102−1−4.

(16) Rykaczewski, K.; Paxson, A. T.; Anand, S.; Chen, X.; Wang, Z.; Varanasi, K. K. Multimode Multidrop Serial Coalescence Effects During Condensation on Hierarchical Superhydrophobic Surfaces. *Langmuir* **2013**, *29*, 881−891.

(17) Lo, C.-W.; Wang, C.-C.; Lu, M.-C. Spatial Control of Heterogeneous Nucleation on the Superhydrophobic Nanowire Array. *Adv. Funct. Mater.* **2013**, *24*, 1211−1217.

(18) He, M.; Zhang, Q.; Zeng, X.; Cui, D.; Chen, J.; Li, H.; Wang, J.; Song, Y. Hierarchical Porous Surface for Efficiently Controlling Microdroplets' Self-Removal. *Adv. Mater.* **2013**, *25*, 2291−2295.

(19) Chen, X.; Wu, J.; Ma, R.; Hua, M.; Koratkar, N.; Yao, S.; Wang, Z. Nanograssed Micropyramidal Architectures for Continuous Dropwise Condensation. *Adv. Funct. Mater.* **2011**, *21*, 4617−4623.

(20) Boreyko, J.; Chen, C.-H. Self-Propelled Dropwise Condensate on Superhydrophobic Surfaces. *Phys. Rev. Lett.* **2009**, *103*, 184501−1−4.

(21) Chen, C.-H.; Cai, Q.; Tsai, C.; Chen, C.-L.; Xiong, G.; Yu, Y.; Ren, Z. Dropwise Condensation on Superhydrophobic Surfaces with Two-Tier Roughness. *Appl. Phys. Lett.* **2007**, *90*, 173108−1−3.

(22) Cheng, J.-T.; Vandadi, A.; Chen, C.-L. Condensation Heat Transfer on Two-Tier Superhydrophobic Surfaces. *Appl. Phys. Lett.* **2012**, *101*, 131909−1−4.

(23) Cheng, Y. T.; Rodak, D. E. Is the Lotus Leaf Superhydrophobic? *Appl. Phys. Lett.* **2005**, *86*, 144101−1−3.

(24) A. Wier, K.; McCarthy, T. J. Condensation on Ultrahydrophobic Surfaces and Its Effect on Droplet Mobility: Ultrahydrophobic Surfaces Are Not Always Water Repellant. *Langmuir* **2006**, *22*, 2433−2436.

(25) Miljkovic, N.; Enright, R.; Wang, E. N. Effect of Droplet Morphology on Growth Dynamics and Heat Transfer During Condensation on Superhydrophobic Nanostructured Surfaces. *ACS Nano* **2012**, *6*, 1776−1785.

(26) Rykaczewski, K.; Osborn, W. A.; Chinn, J.; Walker, M. L.; Scott, J. H. J.; Jones, W.; Hao, C.; Yao, S.; Wang, Z. How Nanorough Is Rough Enough to Make a Surface Superhydrophobic During Water Condensation? *Soft Matter* **2012**, *8*, 8786−8794.

(27) Enright, R.; Miljkovic, N.; Al-Obeidi, A.; Thompson, C. V.; Wang, E. N. Condensation on Superhydrophobic Surfaces: The Role

of Local Energy Barriers and Structure Length Scale. *Langmuir* **2012**, *28*, 14424−144232.

(28) Enright, R.; Miljkovic, N.; Dou, N.; Nam, Y.; Wang, E. N. Condensation on Superhydrophobic Copper Oxide Nanostructures. *J. Heat Transfer* **2013**, *135*, 091304−1−12.

(29) Rykaczewski, K. Microdroplet Growth Mechanism During Water Condensation on Superhydrophobic Surfaces. *Langmuir* **2012**, *28*, 7720−7729.

(30) Miljkovic, N.; Wang, E. N. Condensation Heat Transfer on Superhydrophobic Surfaces. *MRS Bull.* **2013**, *38*, 397−406.

(31) Enright, R.; Miljkovic, N.; Alvarado, J. L.; Kim, K.; Rose, J. W. Dropwise Condensation on Micro- and Nanostructured Surfaces. *Nanoscale Microscale Thermophys. Eng.* **2014**, *18*, 223−250.

(32) Rykaczewski, K.; Scott, J. H. J.; Fedorov, A. G. Electron Beam Heating Effects During Environmental Scanning Electron Microscopy Imaging of Water Condensation on Superhydrophobic Surfaces. *Appl. Phys. Lett.* **2011**, *98*, 093106−1−3.

(33) Miljkovic, N.; Enright, R.; Nam, Y.; Lopez, K.; Dou, N.; Sack, J.; Wang, E. N. Jumping-Droplet-Enhanced Condensation on Scalable Superhydrophobic Nanostructured Surfaces. *Nano Lett.* **2013**, *13*, 179−187.

(34) Li, W.; Amirfazli, A. A Thermodynamic Approach for Determining the Contact Angle Hysteresis for Superhydrophobic Surfaces. *J. Colloid Interface Sci.* **2005**, *292*, 195−201.

(35) Li, W.; Amirfazli, A. Microtextured Superhydrophobic Surfaces: A Thermodynamic Analysis. *Adv. Colloid Interface Sci.* **2007**, *132*, 51−68.

(36) Feng, J.; Qin, Z.; Yao, S. Factors Affecting the Spontaneous Motion of Condensate Drops on Superhydrophobic Copper Surfaces. *Langmuir* **2012**, *28*, 6067−6075.

(37) Dorrer, C.; Rühe, J. Condensation and Wetting Transitions on Microstructured Ultrahydrophobic Surfaces. *Langmuir* **2007**, *23*, 3820−3824.

(38) Yao, C. W.; Alvarado, J. L.; Marsh, C. P.; Jones, B. G.; Collins, M. K. Wetting Behavior on Hybrid Surfaces with Hydrophobic and Hydrophilic Properties. *Appl. Surf. Sci.* **2014**, *290*, 59−65.

(39) Miljkovic, N.; Enright, R.; Wang, E. N. Modeling and Optimization of Superhydrophobic Condensation. *J. Heat Transfer Trans. ASME* **2013**, *135*, 1−14.